PCCP

Accepted Manuscript

This is an *Accepted Manuscript*, which has been through the Royal Society of Chemistry peer review process and has been accepted for publication.

Accepted Manuscripts are published online shortly after acceptance, before technical editing, formatting and proof reading. Using this free service, authors can make their results available to the community, in citable form, before we publish the edited article. We will replace this *Accepted Manuscript* with the edited and formatted *Advance Article* as soon as it is available.

You can find more information about *Accepted Manuscripts* in the Information for Authors.

Please note that technical editing may introduce minor changes to the text and/or graphics, which may alter content. The journal's standard Terms & Conditions and the Ethical guidelines still apply. In no event shall the Royal Society of Chemistry be held responsible for any errors or omissions in this *Accepted Manuscript* or any consequences arising from the use of any information it contains.

ROYAL SOCIETY OF CHEMISTRY

www.rsc.org/pccp

Insight into Photofragment Vector Correlation by Multi-center Impulsive Model

Po-Yu Tsai[*,1] and King-Chuen Lin[*,2]

1. **Department of Chemistry, National Chung Hsing University, Taichung 402, Taiwan**
2. **Department of Chemistry, National Taiwan University, Taipei 106, and Institute of Atomic and Molecular Sciences, Academia Sinica, Taipei 106, Taiwan**

Pages: 31

Figures: 11

*** To whom correspondence should be addressed.**

Email: kclin@ntu.edu.tw and pytsai@dragon.nchu.edu.tw

Physical Chemistry Chemical Physics Accepted Manuscript

Abstract

A multi-center impulsive model has been recently developed to characterize the dynamic feature of product energy distribution in photodissociation of formaldehyde, $H_2CO \rightarrow CO + H_2$. (*J. Phys. Chem. A* 2015,**119**, 29) The model is extended to predict the vector correlations among transition dipole moment μ of the parent molecule, recoil velocity v and rotational angular momentum j of the fragments produced via transition state (TS) and roaming path. The correlation results of μ-j, j-j and μ-v vectors of the fragments are consistent with those reported using quasi-classical trajectory simulation on global potential energy surface. In contrast to the TS route, the vector properties via the roaming path are loosely correlated. This work offers an alternative method to study stereodynamics of photodissociation process, and is conducive to clarifying the origin of photofragment vector correlation especially for roaming pathway.

Physical Chemistry Chemical Physics Accepted Manuscript

1. Introduction

Analysis of the vector properties in molecular photodissociation offers an efficient way to understand the related stereodynamics.[1-5] Information on vector correlations among molecular transition moment, fragment recoil velocity, and fragment angular momentum is conducive to understanding the type of photo-excitation, dissociation lifetime, coherence in electronic state, dissociation mechanisms and the torques generated.[1-15] The photofragment vector correlation was recently inspected to identify the so-called "roaming mechanism"[16-37] in acetaldehyde (CH_3CHO)[16,19] and NO_3 (ref.17,18), but they showed distinctly different features. The photofragment rotational angular momenta of NO_3 along the roaming routes are strongly aligned in recoil frame,[17,18] whereas the photofragments of CH_3CHO possess no significant alignment.[16,19] The roaming trajectories are confined to the NO_3 molecular plane,[17,18] but they become free from any constraint for aldehydes.[16,19-21,32,33,36] As an alternative to the classical or quantum dynamical methods, this work aims to present a simple, generic dynamical model to look into the origin of vector properties especially for the roaming route.

The roaming mechanism that has been explored widely incorporates various processes showing distinct and complicated photofragment energy disposals. Several types of "roaming" were recently suggested[38] to avoid ambiguity in nomenclature. They include (1) dissociation pathways with loose saddle points (SP) found in aldehydes, acetone, alkanes, HOOHO and C_2H_4OH,[16,19-23,25,29,32,33,36] (2) multi-state "reactive funnel" picture[31,37] involving internal conversion (IC) or intersystem crossing (ISC), such as methyl formate, formic acid, and methylamine,[26-28,31,37] (3) isomerization-mediated paths found in nitrobenzene, NO_3 and CH_3NO_2,[17,18,24,30,34] and (4) bimolecular analogues[39-45] including the newly suggested reaction, $OH+HBr \rightarrow H_2O+Br$.[45]

Herein we focus on the photofragment vector correlation of type (1) mechanism characterizing the photodissociation of formaldehyde, $H_2CO \rightarrow CO + H_2$. This reaction scheme serves as a benchmark of both tetratomic molecular photodissociation and roaming mechanism. The vector properties following dissociation via both routes of tight and roaming SP will be examined using an impulsive-based model[46] without involving global potential energy surfaces (PESs). The prior treatments of impulsive

Physical Chemistry Chemical Physics Accepted Manuscript

model are restricted to the cases of only one-bond fission.[47-51] When the reaction is extended to multi-bond breaking/formation processes, the two-center impulsive model becomes insufficient to target such a multi-center problem that requires the information on impulse vectors and relative phase between any two velocity vectors.[47] For this reason, we have recently developed a general multi-center impulsive model to successfully characterize the dynamical feature of the product energy distributions in $H_2CO \rightarrow CO + H_2$ via conventional transition state (TS) and roaming SP pathways.[46]

The vector properties in photodissociation of formaldehyde have been thoroughly investigated. The photofragment angular momentum vectors via the tight SP pathway are perpendicularly aligned with respective to velocity vectors.[47,52,53] Such $v \perp j$ correlation implies that the reaction path is constrained on tetratomic plane and the j vector is parallel with the normal of the tetratomic plane.[16,47,52,53-55] In addition, experimental results suggest that CO and H_2 products favor co-rotation.[47] Such j-j correlation in tight SP pathway is also supported by QCT simulation.[52,53] In contrast, photofragments via roaming trajectories possess no clear $v \perp j$ and j-j correlation[53,55] theoretically, implying that those photofragments are produced via a floppy, unconstrained reaction pathway.[16,53-55]

In this work, we extend the multi-center impulsive model[46] to examine the vector quantities in $H_2CO \rightarrow CO + H_2$, attempting to demonstrate the possibility to predict the photofragment vector correlation. The paper is organized as follows. Section II presents the key concepts of this model and the details about the treatment for vector quantities comprising angular momentum (j), velocity (v) and transition dipole moment (μ). In Section III we analyze the v-j, μ-j, μ-v and j-j correlations associated with both tight SP and roaming pathways. The outcomes are compared with those obtained from previous studies.[52,53] Based on these results, several important issues are raised and discussed, including (1) curvature effect of reaction path, (2) the fate of energy in statistical reservoir,[46,50,51] and (3) the origin of the distinct feature in the roaming vector-correlation of aldehydes. Finally, limitations of the method adopted are summarized.

2. Computational Methods

(A) Photofragment Vector Correlation by Multi-Center Impulsive Model

Physical Chemistry Chemical Physics Accepted Manuscript

The developed multi-center impulsive model[46] relies on the concepts of separated statistical/impulsive reservoirs and hybrid Franck-Condon mapping (FCM)/modified impulsive model (MIM), similarly as the work reported;[50,51] however, this model is capable of tackling the multi-center dissociating process after the following improvement:

(1) The multi-center impulse and torque are determined from *ab initio* Hessian without using additional adjustable parameters.
(2) FCM usually evaluates overlapping integral of vibrational wavefunction,[47,50] but neglects continuum wavefunctions in translational degree of freedom. Such treatment may bring about energy-inaccessible states occurring in a photofragment vibrational distribution, when dealing with vibrational distribution of newly-formed chemical bond(s) and its photolysis-wavelength dependence.[46] For this reason, with the aid of internal energy distribution predicted from (1), an energy-weighing procedure (denoted as energy-weighted Franck-Condon mapping (EWFCM) in ref 46) was considered to eliminate the shortcomings.
(3) In order to remain momentum conservation without causing any unreasonable energy flow between photofragments, the fragmentary rigid impulsive (FRI) scheme[46] is adopted to replace conventional rigid impulsive scheme (MIM).[47-51]
(4) The zero-point vibrations of parent molecule are explicitly considered to provide distributions of scalar properties in either position or momentum domain.[46]

Basing on the procedure described previously,[46] this work aims to predict the vector properties of photofragments involving the effect of parent molecular vibration in both position and momentum domain. Further, instead of using an analytical distribution function, the rotational angular momentum is evaluated by vector addition between multi-center impulse and zero-point vibration. The rotational state-averaged vector properties of photofragments are obtained as follows. First, determine the atomic displacements and atomic velocity variation which are caused by zero-point vibrations. Then, calculate the vector properties, and finally, analyze the correlation between vector properties. The zero-point vibrations of the real parent modes at critical geometry are sampled by using Wigner distribution function (for example, see ref.56). The quasi-classical momentum (p_i) and position (q_i) distributions of N

Physical Chemistry Chemical Physics Accepted Manuscript

harmonic oscillators in its vibrational ground state can be represented in terms of Wigner distribution.[56]

$$P_W\left(q_1, p_1, \ldots, q_N, p_N\right) = \prod_{i=1}^{N} W\left(q_i, p_i\right)$$
$$W\left(q_i, p_i\right) = \frac{1}{\pi\hbar} e^{-m_i\omega_i q_i^2/\hbar} e^{-p_i^2/(m_i\omega_i\hbar)} \quad \textbf{(1)}$$

where W is the ground state Wigner distribution function (WDF) of one-dimensional harmonic oscillator, ω_i and m_i are angular frequency and mass of i-th harmonic oscillator, respectively. The atomic velocities caused by zero-point vibrations are vector-added to the velocities from impulse in the frame of Cartesian coordinate. Geometric variations resulting from zero-point vibrations are taken into account similarly by adding atomic displacements to the molecular equilibrium geometry. A set of totally 2×(3N-7) random numbers is required to represent a point on 2×(3N-7) dimensional phase space which describes the vibrational motion of an N-atomic nonlinear molecule at its saddle point configuration. The atomic positions and momenta as sampled from 10^4 random number sets are then used to evaluate the distributions of vector properties including the bond axes of parent molecule, velocities and angular momenta of photofragments. The rotational angular momentum vector of an n-atomic photofragment is calculated classically in center-of-mass (c.m.) frame of photofragment by

$$\vec{j} = \sum_n \vec{r}_n \times \vec{p}_n \quad \textbf{(2)}$$

The vector correlation can be readily determined following the distribution of vector properties. Four types of photofragment vector correlations are demonstrated for the scheme, $H_2CO \rightarrow H_2+CO$, including (1) photofragment v-j correlation, (2) photofragment μ-j correlation, (3) μ-v correlation, and (4) j-j correlation between two photofragments. This study considered only the available energy contained in the impulsive reservoir[46,50,51] of each pathway. Impulsive reservoir is defined as the energy difference between the critical geometry and the product (zero-point energy is included.). Its value is estimated by summing the reaction exoergicity of 759 cm^{-1} and the threshold energy of 27720 cm^{-1} (ref.57,58) for tight SP pathway or 30180cm^{-1} (ref.59) for roaming pathway.[57,58] This study presents only the state-averaged results based on the photofragment rovibrational distribution reported[46] and the

Physical Chemistry Chemical Physics Accepted Manuscript

photofragment angular momentum distributions are counted in statistic without additional constraint of j vector norm.

(B) ab initio Electronic Structure Calculation of $H_2CO \rightarrow H_2+CO$

All the single-reference and multi-reference electronic structure calculations in this study are performed via GAMESS electronic structure package.[60,61] The geometry of roaming SP of $H_2CO \rightarrow H_2+CO$ is optimized at (8e,8o)-MRMP2/aug-cc-pVDZ level.[62] The intrinsic reaction coordinate (IRC)[63] and vibrational frequencies of five real parent modes along the reaction path[64] are calculated at the same level. For tight SP, the geometry and vibrational frequencies are calculated by using CR-CC(2,3) method[65,66] with aug-cc-PVTZ basis function. In addition, in order to clarify the discrepancy between the QCT results[52] and the impulsive approach, MP2 method with aug-cc-PVDZ basis set is also utilized for the tight SP pathway.

3. Results and Discussion

(A) Tight Saddle Point Pathway

Miller and co-workers performed QCT calculations[52] for the H_2CO photodissociation on an accurate global PES that was constructed based on empirical valence-bond model. Given the assumption of prompt photodissociation, the classical trajectories were initiated at the tight SP with an excess energy of 1800 cm^{-1} (above zero-point energy (ZPE) level) deposited in imaginary mode.[52] As a result, they found a series of significant vector correlations: such as, H_2CO breaking into H_2 + CO is on a near-planar structure, the recoil velocity of CO is aligned perpendicular to both the transition dipole moment and its rotational angular momentum, and the alignment of j_{H2} and j_{CO} favors co-rotation. In order for comparison with the QCT results,[52] we adopt the same definition of the coordinate for the tight TS geometry. That is, for a near planar SP structure, transition dipole moment μ is parallel to the b axis of the molecular frame,[52] given the assumption that the formaldehyde excited states such as $2^1 4^1$ and others probed by Moore and coworkers belong to a b-type transition.[47,52,67,68] This b axis is almost perpendicular to the CO bond and lies on the molecular plane. On the other hand, the photofragment recoil velocity v in the molecular frame following a prompt dissociation of H_2CO is defined by the polar angle θ_v and

Physical Chemistry Chemical Physics Accepted Manuscript

azimuthal angle ϕ_v. Similarly, the fragment rotational angular momentum j is defined by θ_j and ϕ_j in recoil frame. Fig.1(a) displays the coordinate for transition state geometry and fragment.

The correlations among μ, v and j vectors are evaluated and compared with those reported.[52] As shown in Fig.2, a plot of the v-j polar angle θ_{CO} and θ_{H2} for the CO and H_2 fragments yields 90°, indicating v is perpendicular to j. The recoil velocities of CO and H_2 lie in the tight SP plane, while their individual rotational angular momentum is perpendicular to this plane. As compared to the CO distribution (Fig.2a), the H_2 polar angle spreads from 30° to 150° (Fig.2b). The impulsive results are consistent with those by the QCT method, except that the QCT plot of H_2 polar angle shows a symmetric doublet with respect to the central peak.

Fig.3 shows the μ-j polar- and azimuthal-angle dependence of the CO production distribution. The former dependence peaks at 90°, indicating that the transition dipole moment is perpendicular to the CO rotational angular momentum. The μ-j azimuthal angle distribution peaking at 0° reflects that the j is parallel to the normal of the tetratomic plane (yz plane in Fig1(a)), consistent with the prediction in Fig.2. Similarly, for the H_2 fragment the μ-j polar angle distribution peaks at 90°, as shown in Fig.4, and thus j is anticipated to be perpendicular to μ. However, the azimuthal angle dependence spreads widely peaking at 0° or 360°, suggesting that j_{H2} be dominated by the parallel alignment with respect to the plane normal. The coupling with out-of-plane vibrational mode during the moment of photodissociation results in azimuthal angle variation. The evaluation by impulsive model is essentially consistent with the QCT prediction, except that a doublet μ-j polar angle distribution was obtained previously, different from a peak distribution in this work. As for the j-j correlation, Fig.5 shows that the CO and H_2 rotational angular momentum favor co-rotation, despite a wide angle variation between j_{CO} and j_{H2}. The trend for the j-j correlation is reasonable, because the J_{CO} lies in parallel with the normal of the tetratomic plane, but the j_{H2} lies at a varied angle with respect to the plane normal. The results are also consistent with the QCT prediction.

The μ-v_{CO-H2} correlation in which v_{CO-H2} is the relative recoil velocity of the CO-H_2 products is analyzed, despite observation hindrance by parent rotation.[20] Miller and coworker[52] obtained a μ- v_{CO-H2} polar angle distribution from 20 to 50° peaking at 40° using the CCSD PES, and thus the parallel transition is anticipated to

Physical Chemistry Chemical Physics Accepted Manuscript

prevail slightly. A narrow azimuthal angle distribution peaks at 270°, suggesting a near-planar molecular dissociation for $H_2CO \rightarrow H_2 + CO$. In comparison, as shown in Fig.6(a), the present work predicts the azimuthal angle of 270°, consistent with the QCT results, despite a slightly larger width. However, the impulsive model predicts the polar angle dependence peaking at 30° with the profile shifted to a smaller angle region (Fig.6(b)). The discrepancy may be explained in the following. The impulsive model assumes that an impulse exerted on the TS configuration results in the rupture of two fragments along a straight line. Such extrapolation of gradient is valid only when the curvature of reaction coordinate on PES is negligible. In fact, the minimum energy path could be curved.[64,69] The curvature along the reaction coordinate should be mainly responsible for the discrepancy, given that the sudden approximation is valid for the impulsive model.

Despite the success in predicting photofragment rotational state distributions,[46,47,70] how to take into account the curvature effect in the impulsive model becomes challenging. As shown in Fig.7(a), the IRC dependent energy and the corresponding gradient profile of the tight SP pathway (toward the product side) are evaluated at MP2/aug-cc-pVDZ level (Fig.7(a)). The scalar and vector properties of atomic acceleration at each IRC point are thus obtained by analyzing the atomic gradients. Fig.7(b) shows the fraction of CO rotational excitation and the directional variation of photofragment translational acceleration vectors. The results imply the following aspects. (1) Direction of relative velocity vector (v) of photofragment changes with respect to the molecular frame. Such variation is expressed by monitoring the change of polar angle between transition dipole moment (μ) and the translational acceleration vector of CO. The fragment translational acceleration vector rotates about 18° on the yz plane, due to the curvature of reaction coordinate (red curve in Fig.7(b)). (2) Meanwhile, the fragment rotational acceleration vector rotates simultaneously on the yz plane. (3) Accordingly, v-j correlation is invariant with the curvature of reaction coordinate and thus can be successfully predicted herein. (4) The fraction of CO rotational excitation in acceleration remains almost constant (14%~11%) along the reaction coordinate. In contrast, the direction of relative velocity vector (v) of photofragment changes with respect to transition dipole moment (μ) which is fixed in molecular frame. The curvature effect changes the directions of photofragment rotational/translational acceleration vectors, but leaves the vector norms (almost) unchanged (red curve in Fig.7(b)). That is why the impulsive models

Physical Chemistry Chemical Physics Accepted Manuscript

can precisely predict photofragment energy distribution along the tight SP pathway and the v-j correlation, irrespective of the curvature effect.

As for the μ-v_{CO-H2} angle deviation, we propose the following method to improve the impulsive results. This treatment is valid as long as the curvature effect behaves likely as a rotation of the acceleration vectors in three-dimensional space, with the vector norms being preserved. In the tight SP pathway, the treatment further assumes a simultaneous rotation of the translational and rotational acceleration vectors of photofragments without change of their lengths. Then, the following steps are taken to correct the μ-v_{CO-H2} correlation. (1) Obtain the vector distributions by impulsive model. (2) Perform a classical trajectory simulation initiated on the minimum energy path (MEP). In practice, the *ab initio* "on the fly" dynamic is applied starting at a SP configuration with a little kinetic energy (0.1 kcal/mol, ca.35 cm^{-1}) on the imaginary mode. (3) Determine the rotational angles (Ω) for the three-dimensional vector rotation. In this work, the rotational angle is defined as the angle between initial and final relative velocity vectors of photofragments (v_{H2-CO}). The initial velocity is determined based on the imaginary mode of the tight SP, and the final velocity is obtained from asymptotic velocity vector of the trajectory. (4) Rotate the whole relative velocity vector distribution by the same angle (Ω) and thus obtain the μ-v_{H2-CO} correlation. The corrected polar angle distribution becomes consistent with the QCT calculation, although the profile width is wider. For each vector property, the above improvement introduces only an extra parameter (Ω) which is provided by a classical trajectory along MEP. Its validity requires that the curvature effect of reaction coordinate does not alter the scalar properties of PED, i.e., the norm of vector is preserved. In terms of such an "elastic curvature approximation", the capability of impulsive model is expanded to characterize the vector properties of PED.

Some distributions of vector correlations by Miller and coworkers[52] yield a symmetric doublet such as v-j and μ-j correlation of H_2 and μ-j correlation of CO, whereas the corresponding results by impulsive model usually show a peak profile. Such doublet may be attributed to the effect of out-of-plane bending mode (ν_4) which is known to be responsible for the width of v-j correlational distribution. Fig.8 shows the position probability distribution of the ν_4 mode at v=0-2 states. In vibrational excited states, the most probable molecular structure possesses doublet and tends to be non-planar, therefore the directions of v and j vectors deviate to v' and j' from the

Physical Chemistry Chemical Physics Accepted Manuscript

tetratomic plane (yz) and its normal axis, respectively. In addition, Fig.8 illustrates how the v and j vector properties vary simultaneously with the vibrational motion. Thus, the v-j doublet structure becomes less pronounced in the QCT results (Fig.2). In the QCT calculations,[52] five real vibrational modes at tight SP configuration were set at the zero-point energy state and the excess energy about 1800 cm^{-1} was deposited to the imaginary mode along the reaction coordinate. Therefore, the doublet character in the vector correlation plots may be caused by the ν_4 mode excitation (877 cm^{-1} obtained from CR-CC(2,3) computation) through the coupling between reaction coordinate and transverse modes. It is well known that such coupling is driven by the curvature of reaction path.[64,69]

(B) *Roaming Saddle Point Pathway*

Unlike the tight SP, the roaming SP is far from the condition of sudden limit and thus the impulsive model cannot work properly. As reported previously,[46] the product energy disposal (PED) via roaming pathway has been examined by varying molecular configurations along the edge of the plateau-like IRC. The obtained PED results appear similar to each other, but the configuration C3 defined in the previous paper[46] yields the minimum translational energy and shows quantitative consistency with the experimental results.[20] Thus, this configuration is selected as the critical geometry to evaluate the vector quantities in this work (Fig.1(b)). Different from the tight SP with a planar structure, this configuration possesses chirality (see Fig.1(b)) and thus the following simulation takes into account two enantiomers with equivalent contribution. Fig.9 shows a v-j polar angle distribution, in comparison with the corresponding correlation via the tight SP pathway. The v-j polar angles of H_2 fragment peak around 70°-110° with a wider spread of the angle distribution for the roaming mechanism. For the CO fragment, a much wider polar angle distribution is found in contrast to a very narrow distribution via tight SP mechanism. Further, double maxima which are ascribed to the two chiral enantiomers can be observed, peaking at 60° and 120°. We expect that the doublet feature may be smashed, if anharmonicity is included in the treatment that should result in further scrambling of the angle distribution. Because roaming follows a more floppy reaction route, the recoil velocity and the rotational angular momentum are loosely correlated with respect to the tight SP route. Further, while examining the μ-v correlation, Fig.10 shows the azimuthal angle dependence

Physical Chemistry Chemical Physics Accepted Manuscript

that yields the maximum population at either 20^0 or 340^0, favoring H_2CO dissociation out of the molecular surface. On the other hand, the polar angle distribution shows the maximum population around 75^0 -105^0, suggesting that the fragments are produced in a large phase space. While combining the polar angle and the azimuthal angle distributions, the fragments produced via the roaming pathway occupy a much larger velocity vector space than that generated by the tight SP pathway. The results again reveal the floppy nature of roaming pathway. The j-j polar angle distribution is also inspected in Fig.11, showing the maximum population around 70°-110°, indicating that CO and H_2 rotational angular momentum tend to be slightly perpendicular to each other, in contrast to co-rotation behavior dominated along the tight SP pathway. By comparing with the QCT result[53] of H_2 fragment with v_{HH} >4 which stems mainly from the roaming route, the trend is consistent except for the two regions at >160° and <20°. Again, the discrepancy may be attributed to the neglect of anharmonicity in our impulsive treatment.

Our impulsive model not only reproduces the distinct features of vector correlations for the two pathways, but also provides new insight into the "roaming signature" in photofragment vector properties. Despite lack of the vector correlation experiments found in H_2CO via the roaming pathway, the loose v-j correlation along the roaming pathway was widely recognized as the consequence of the delayed, randomized fragment-reorienting motion.[16,20,21,33,35,53-55,70-72] However, we offer an alternative interpretation based on the analysis of model calculations. Impulsive models[46-51] predict the dynamical behavior via the impulse at a critical geometry (see Fig.1(b)), which is fixed at the edge of the plateau-like IRC, without discerning how the molecules evolve to it. Accordingly, the loose vector correlation simulated by the impulsive model does not depend on the floppy, roaming motion. Instead, the vector properties different from the tight SP route are strongly influenced by the floppy transverse vibrational motions which are perpendicular to the gradient at critical geometry. In short, the distributions of photofragment vector properties (j vector as example) are governed essentially by the norms of impulse and transverse vibrations,[46] $\vec{j}_{TOT} = \vec{j}_{IMP} + \vec{j}_{ZP}$. A larger impulse norm (j_{IMP}) results in a narrower spread of the total vectors (j_{TOT}), whereas a larger zero-point vibration norm (j_{ZP}) results in a wider spread. The photofragment velocity and angular momentum vectors via a roaming route show the following features: (1) a short CO j_{IMP} because of low

Physical Chemistry Chemical Physics Accepted Manuscript

rotational excitation by impulse, (2) a short H_2 j_{IMP} because of most excess energy flow into H_2 vibration, (3) a short v_{IMP} because of low translational excitation by impulse, and (4) a long j_{ZP} because of large variation on molecular geometries by low-frequency modes. Accordingly, the above effects lead to broader, loosely correlated vector distributions.

(C) Limitation of Impulsive Model

Despite simplicity and capability in predicting photofragment vector correlation, several limitations of this treatment cannot be ignored. (1) The separated statistical/impulsive reservoirs[50,51] are adopted in this model, but the validity of such assumption to vector quantities remains unknown. This work focuses on impulsive reservoirs and the effect of statistical reservoir is not examined. (2) This method highly relies on the IRC construction along which configurations with the dividing surfaces are located. Thus, the reaction path must be known. (3) The validity of sudden approximation is required. (4) The local PES construction for impulsive reservoir and state counting in statistical reservoir (not examined in this work) are based on harmonic approximation. Anharmonicity of parent molecular vibrations is not considered. (5) As mentioned above, curved reaction path may sometimes be dealt with.

4. Conclusion

A multi-center impulsive model is extended to analyze the photofragment vector correlation of the reaction, $H_2CO \rightarrow CO + H_2$. Alternative to the QCT calculations on a global PES, the model is capable of reproducing consistent trends of the photofragment vector correlations especially via a tight SP pathway. The outcome allows us to characterize stereodynamic behavior of the reaction and to gain deep insight into the origin of vector properties. The loose vector correlation along the roaming pathway was popularly recognized as a result of the delayed, randomized fragment-reorienting motion. Nevertheless, the impulsive model predicts such dynamical behavior via the impulse at a selected configuration along the plateau-like IRC without the knowledge of molecular evolution. The characterization of vector distribution seems to be less influenced by the roaming motion. Instead, we propose

Physical Chemistry Chemical Physics Accepted Manuscript

that the floppy photofragment vector correlation in formaldehyde via the roaming pathway should be attributed to a combined effect occurring at the critical geometry from which (1) the low rotational excitation is generated by the impulse, in significant coupling with (2) the low-frequency parent vibrations perpendicular to the reaction coordinate.

Acknowledgement

This work is supported by Ministry of Science and Technology of Taiwan, Republic of China under contract no. NSC 102-2113-M-002-009-MY3.

Physical Chemistry Chemical Physics Accepted Manuscript

References

1. R. N. Dixon, *J. Chem. Phys.* 1986,**85**, 1866-1879.
2. P. L. Houston, *J. Phys. Chem.* 1987, **91**, 5388-5397.
3. L. D. A. Siebbeles, M. Glass-Maujean, O. S. Vasyutinskii, J. A. Beswick and O. Roncero, *J. Chem. Phys.*, 1994, **100**, 3610-3623.
4. T. P. Rakitzis and R. N. Zare, *J. Chem. Phys.* 1999, **110**, 3341-3350.
5. A. G. Suits and O. S. Vasyutinskii *Chem. Rev.* 2008,**108**, 3706-3746.
6. G. G. Balint-Kurti, A. J. Orr-Ewing, J. A. Beswick, A. Brown, and O. S. Vasyutinskii, *J. Chem. Phys.*, 2002,**116**, 10760-10768.
7. V. V. Kuznetsov and O. S. Vasyutinskii, *J. Chem. Phys.*, 2005,**123**, 034307.
8. V. V. Kuznetsov and O. S. Vasyutinskii, *J. Chem. Phys.* 2007,**127**, 044308.
9. P. S. Shternin and O. S. Vasyutinskii, *J. Chem. Phys.* 2008, **128**, 194314.
10. V. V. Kuznetsov, P. S. Shternin, and O. S. Vasyutinskii, *J. Chem. Phys.* 2009,**130**, 134312.
11. T. P. Rakitzis and A. J. Alexander, *J. Chem. Phys.* 2010,**132**, 224310.
12. T. P. Rakitzis, *J. Chem. Phys.* 2010,**133**, 204301.
13. M. B. Krasilnikov , V. V. Kuznetsov, A G. Suits, and O. S. Vasyutinskii, *Phys. Chem. Chem. Phys.*, 2011,**13**, 8163-8174.
14. L Bougas and T. P. Rakitzis, *Phys. Chem. Chem. Phys.* 2011, **13**, 8526-8530.
15. P. S.Shternin, A. G.Suits, O. S. Vasyutinskii, *Chem. Phys.* 2011, **399**, 162-171.
16. P. L. Houston and S. H. Kable, *Proc. Natl. Acad. Sci. USA*, 2006, **103**, 16079-16082.
17. M. P. Grubb , M. L. Warter, and S. W. North, *Phys. Chem. Chem. Phys.* 2012, **14**, 6733-6740.
18. M. P. Grubb, M. L. Warter, H. Xiao, S. Maeda, K. Morokuma,S. W. North *Science* 2012,**335**,1075-1078.
19. K. L. K. Lee, M. S. Quinn, A. T. Maccarone, K. Nauta, P. L. Houston, S. A. Reid, M. J. T. Jordan, and S. H. Kable, *Chem. Sci.* 2014,***5***, 4633-4638.
20. D. Townsend, S. A. Lahankar, S. K. Lee, S. D. Chambreau, A. G. Suits, X. Zhang , J. Rheinecker, L. B. Harding, and J. M. Bowman, *Science*, 2004, **306,** 1158-1160.
21. B. R. Heazlewood, M. J. T. Jordan, S. H. Kable, T. M. Selby, D. L. Osborn, B. C. Shepler, B. J. Braams, and J. M. Bowman, *Proc. Nat. Acad. Sci. USA* 2008,**105**,

Physical Chemistry Chemical Physics Accepted Manuscript

12719-12724.

22. L. B. Harding, and S. J. Klippenstein, *J. Phys. Chem. Lett.* 2010, **1**, 3016-3020.
23. E. Kamarchik, L. Koziol, H. Reisler, J.M. Bowman, and A.I. Krylov, *J. Phys. Chem. Lett.* 2010, **1**, 3058-3065.
24. M.L. Hause, N. Herath, R. Zhu, M.C. Lin, and A.G. Suits, *Nat. Chem.* 2011, **3**, 932-937.
25. L. Rubio-Lago, G. A. Amaral, A. Arregui, J. Gonzalez-Vazquez, and L. Banares, *Phys. Chem. Chem. Phys.* 2012,**14**, 6067-6078.
26. J.O. Thomas, K.E. Lower, and C. Murray, *J. Phys. Chem. Lett.* 2012, **3**, 1341-1345.
27. S. Maeda, T. Taketsugu, and K. Morokuma, *J. Phys. Chem. Lett.* 2012, **3**, 1900-1907.
28. H. Xiao, S. Maeda, and K. Morokuma, *J. Phys. Chem. A* 2013, **117**, 5757-5764.
29. A. Matsugi, *J. Phys. Chem. Lett.* 2013, **4**, 4237-4240.
30. Z. Homayoon and J.M. Bowman, *J. Phys. Chem. A* 2013,**117**, 11665-11672.
31. P.-Y. Tsai, M.-H. Chao, T. Kasai, K.-C. Lin, A. Lombardi, F. Palazzetti and V. Aquilanti, *Phys. Chem. Chem. Phys.*, 2014, **16**, 2854-2865.
32. K.-C. Hung, P.-Y. Tsai, H.-K. Li and K.-C. Lin, *J. Chem. Phys.*, 2014, **140**, 064313
33. P.-Y. Tsai, K.-C. Hung, H.-K. Li and K.-C. Lin, *J. Phys. Chem. Lett.*, 2014,**5**,190-195.
34. A. Dey, R. Fernando, C. Abeysekera, Z. Homayoon, J.M. Bowman and A.G. Suits, *J. Chem. Phys.* 2014, **140**, 054305.
35. J. M, Bowman, Roaming, *Mol. Phys.*,2014,**112**, 2516-2528.
36. H.-K. Li, P.-Y. Tsai, K.-C. Hung, T. Kasai, and K.-C. Lin, *J. Chem. Phys.*,2015,**142**,041101.
37. M. Nakamura, P.-Y. Tsai, T. Kasai, K.-C. Lin, F. Palazzetti, A. Lombardi and V. Aquilanti, *Faraday Discuss.*, 2015,**177**, 77-98.
38. K. Dhoke, *et. al. Faraday Discuss.*, 2015, **177**, 121-154.
39. J. Mikosch, S. Trippel, C. Eichhorn, R. Otto, U. Lourderaj, J. X. Zhang, W. L. Hase, M. Weidemuller, R. Wester, *Science*, 2008,**319**,183-186.
40. K.M. Christoffel and J.M. Bowman, *J. Phys. Chem. A* 2009,**113**, 4138-4144.
41. Á. Bencsura and G. Lendvay, *J. Phys. Chem. A* 2012,**116**, 4445-4456.
42. H.-G. Yu, *Phys. Scr.* 2011,**84**, 028104.

Physical Chemistry Chemical Physics Accepted Manuscript

43. T. Takayanagi and T. Tanaka, *Chem. Phys. Lett.* 2011,**504**, 130-135.
44. A. Li, J. Li, and H. Guo, *J. Phys. Chem. A* 2013,**117**, 5052-5060.
45. N. D. Coutinho, V. H. C. Silva, H. C. B. de Oliveira, A. J. Camargo, K. C. Mundim, and V. Aquilanti, *J. Phys. Chem. Lett.* 2015,6,1553-1558.
46. P. -Y. Tsai, and K. C. Lin *J. Phys. Chem. A* 2015,**119**, 29-38.
47. T. J. Butenhoff, K. L. Carleton, and C. B. Moore, *J. Chem. Phys.* 1990, **92**, 377-393.
48. G. E. Busch and K. R. Wilson, *J. Chem. Phys.*, 1972, **56**, 3626-3638.
49. A. F. Tuck, *J. Chem. Soc., Faraday Trans 2*,1977,**73**, 689-708.
50. D. H. Mordaunt, D. L. Osborn and D. M. Neumark, *J. Chem. Phys.* 1999,**108**, 2448-2457.
51. S. W. North, D. A. Blank, J. D. Gezelter, C. A. Longfellow and Y.-T. Lee, *J. Chem. Phys.,*1995, **102**, 4447-4460.
52. Y. T. Chang, C. Minichino, and W. H. Miller, *J. Chem. Phys.* 1992, **96**, 4341-4355.
53. J. D. Farnum, X. Zhang, and J. M. Bowman, *J. Chem. Phys.* 2007, **126**, 134305.
54. J.L. Rheinecker , X. Zhang and J.M. Bowman, *Mol. Phys.* 2005,**103**,1067-1074.
55. B. C. Shepler, B. J. Braams, and J. M. Bowman, *J. Phys. Chem. A*, 2007, **111**, 8282-8285.
56. B. Fu, S. C. Shepler, J. M. Bowman , *J. Am. Chem. Soc.*, 2011, **133** , 7957-7968.
57. R. D. van Zee, M. F. Foltz, C. B. Moore, *J. Chem. Phys.*1993*,* **99**, 1664-1673.
58. S. A. Lahankar, S. D. Chambreau, D. Townsend, D. Suits, J. Farnum, X. Zhang, J. M. Bowman, A. G. Suits, *J. Chem. Phys.*, 2006,**125***,* 044303.
59. D. U.Andrews, S. H. Kable, M. J. T. Jordan, *J. Phys. Chem. A* 2013, **117***,* 7631-7642.
60. M. W. Schmidt, K. K. Baldridge, J. A. Boatz, S. T. Elbert, M. S. Gordon, J. H. Jensen, S. Koseki, N. Matsunaga, K. A. Nguyen, S. J. Su, T. L. Windus, M. Dupuis, J. A. Montgomery, *J. Comput. Chem.* **1993***,14*, 1347-1363.
61. M. S. Gordon and M. W. Schmidt in *Theory and Applications of Computational Chemistry: The First Forty Years,* ed. *C. E.*Dykstra, G. Frenking, K. S. Kim, G.E. Scuseria, Elsevier: Amsterdam, **2005**; pp. 1167–1190
62. H. Nakano, *J. Chem. Phys.* **1993**, *99*, 7983-7992.
63. C. Gonzalez and H. B. Schlegel, *J. Chem. Phys.,* **1989**, 90, 2154-2161.
64. W. H. Miller, N. C. Handy, J. E. Adams, *J. Chem. Phys.***1980***,72,* 99-112.

Physical Chemistry Chemical Physics Accepted Manuscript

65. P. Piecuch, S. A. Kucharski, K. Kowalski, M. Musial, *Comput. Phys. Commun.* **2002**,*149*,71-96.
66. P. Piecuch, M. Wloch, *J. Chem. Phys.* **2005**,*123*, 224105.
67. K. L. Carleton, T. J. Butenhoff, and C. B. Moore, *J. Chem. Phys.* 1990,**93**, 3907-3918.
68. T. J. Butenhoff, K. L. Carleton, R. D. van Zee, and C. B. Moore, *J. Chem. Phys.* 1990,**94**, 1947-1953.
69. M. Page and J. W. McIver, *J. Chem. Phys.,* 1988,**88**, 922-935.
70. S. D. Chambreau, S. A. Lahankar, and A. G. Suits, *J. Chem. Phys.* 2006, **1**25,044302
71. A. G. Suits, *Acc. Chem. Res.* 2008, **41**, 873-881.
72. J. M. Bowman and B. C. Shepler, *Annu. Rev. Phys. Chem.* 2011, **62**, 531-553.

Physical Chemistry Chemical Physics Accepted Manuscript

Figure Captions

Fig.1 The vector quantities of parent molecule and photofragments: transition dipole moment μ, velocities(v_{CO}, v_{HH}), and rotational angular momentum (j_{CO}, j_{HH}) , and the definition of molecular frame for critical geometry of each pathway. (a) tight saddle point with vibrational displacements of imaginary mode (red arrows). The transition dipole moment μ is along the b axis and four atoms are located on the molecular plane (yz). (b) geometry selected for roaming pathway(see text). Yellow arrows represent the direction and relative magnitudes of the atomic acceleration vectors calculated from gradient.

Fig.2 v-j correlation for (a) CO and (b) H_2 fragments. The QCT result was adopted from ref.52.

Fig.3 μ-j correlation for CO fragment. (a) polar angle distribution, and (b) azimuthal angle distribution. The polar angle is defined as the angle between transition dipole moment μ (z axis) and j vector of CO, while the azimuthal angle is defined on xy plane with the positive x direction set as zero. The QCT result was adopted from ref.52.

Fig.4 μ-j correlation for H_2 fragment. (a) polar angle distribution, and (b) azimuthal angle distribution. The polar and azimuthal angles have the same definition as in Fig.3. The QCT result was adopted from ref.52.

Fig.5 The distribution of polar angle between rotational angular momentum vectors j_{CO} and j_{H2} (the j-j correlation). The QCT result was adopted from ref.52.

Fig.6 (a) azimuthal angle distribution between the transition dipole moment μ and the relative velocity $v_{H2\text{-}CO}$ of the H_2-CO products. (b) polar angle distribution between μ and $v_{H2\text{-}CO.}$ The impulsive results are predicted with and without curvature effect included (see text). The QCT result was adopted from ref.52.

Fig.7 Intrinsic reaction coordinate (IRC) of tight SP pathway by MP2/aug-cc-pVDZ calculation. (a) Energy (red) and gradient magnitude (black); (b) Fraction of CO rotational excitation (red) and the polar angle (black) between transition dipole moment (μ) and the acceleration vector of CO translation which is evaluated from gradient at each IRC point.

Fig.8 Effect of ν_4 out-of-bending mode (877 cm^{-1}). The probability density distributions of harmonic wavefunctions (v=0-2) are plotted versus normal mode

Physical Chemistry Chemical Physics Accepted Manuscript

coordinate. In vibrational excited states, the most probable molecular structure is no longer planar and possesses doublet, therefore the directions of v and j vectors deviate to v' and j' from the tetratomic plane (yz) and its normal axis, respectively. The net effect of such vibrational excitation is to form doublet in μ-v and μ-j correlation, but not v-j correlation, since the v, j vectors deviate simultaneously (v→v', j→j').

Fig.9 v-j correlation of (a) H_2 and (b) CO fragments produced via roaming path. The correlation via the tight SP mechanism calculated from QCT and impulsive methods are included for comparison.

Fig.10 (a) azimuthal angle distribution between the transition dipole moment μ and the relative velocity $v_{H2\text{-}CO}$ of the H_2-CO products obtained via roaming path. (b) polar angle distribution between μ and $v_{H2\text{-}CO}$ via roaming path. The spatial distributions via the tight SP pathway calculated from QCT and impulsive methods are included for comparison. QCT result was adopted from ref.52.

Fig.11 polar angle distribution between CO rotational angular momentum j_{CO} and H_2 rotational angular momentum j_{H2} via the roaming path. The QCT results initiated from tight SP geometry (ref.52) and equilibrium geometry(ref.53), and our impulsive method are included for comparison.

Physical Chemistry Chemical Physics Accepted Manuscript

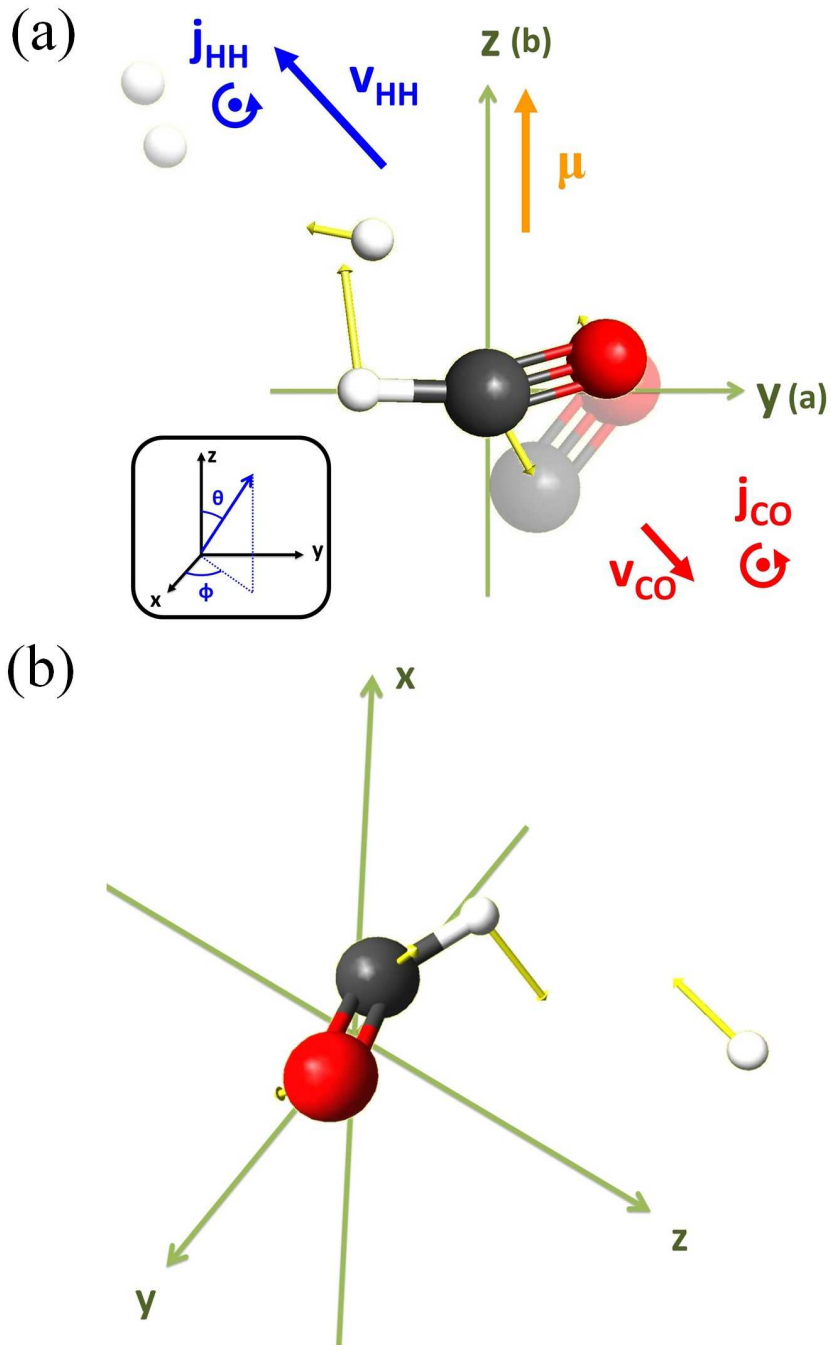

Fig.1

Physical Chemistry Chemical Physics Accepted Manuscript

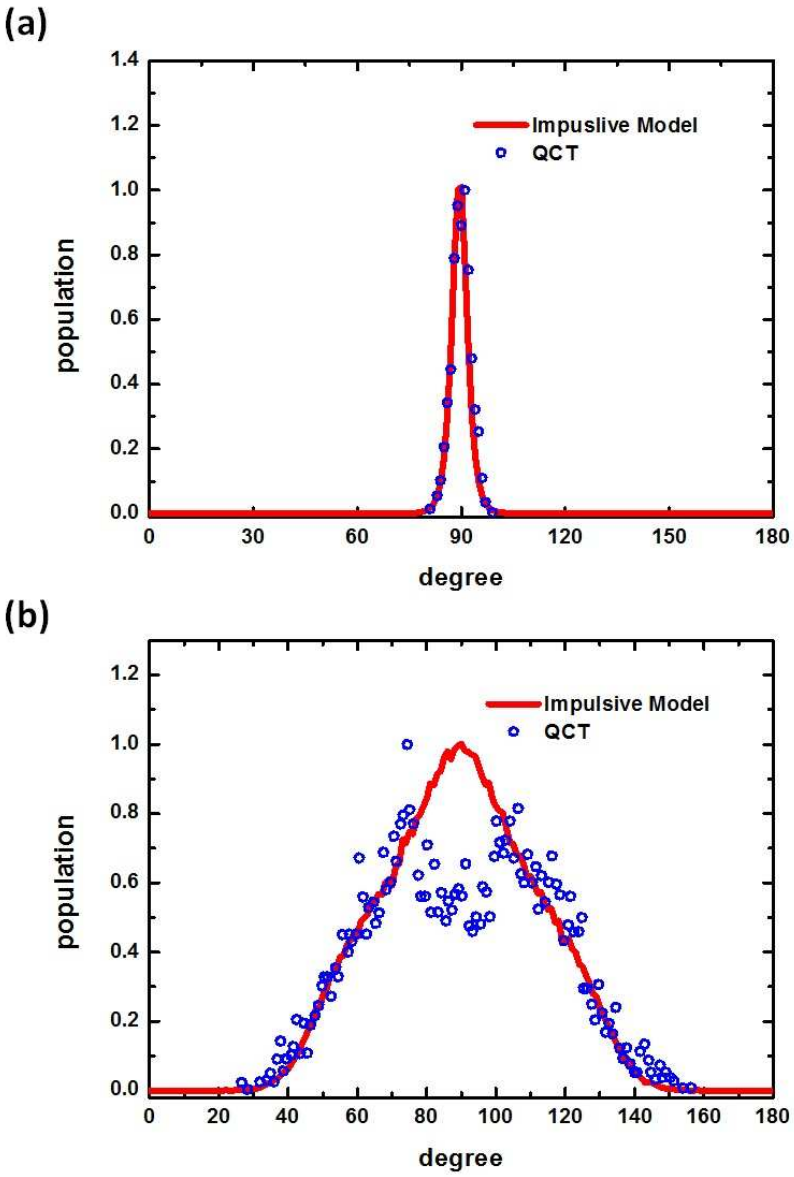

Fig.2

Physical Chemistry Chemical Physics Accepted Manuscript

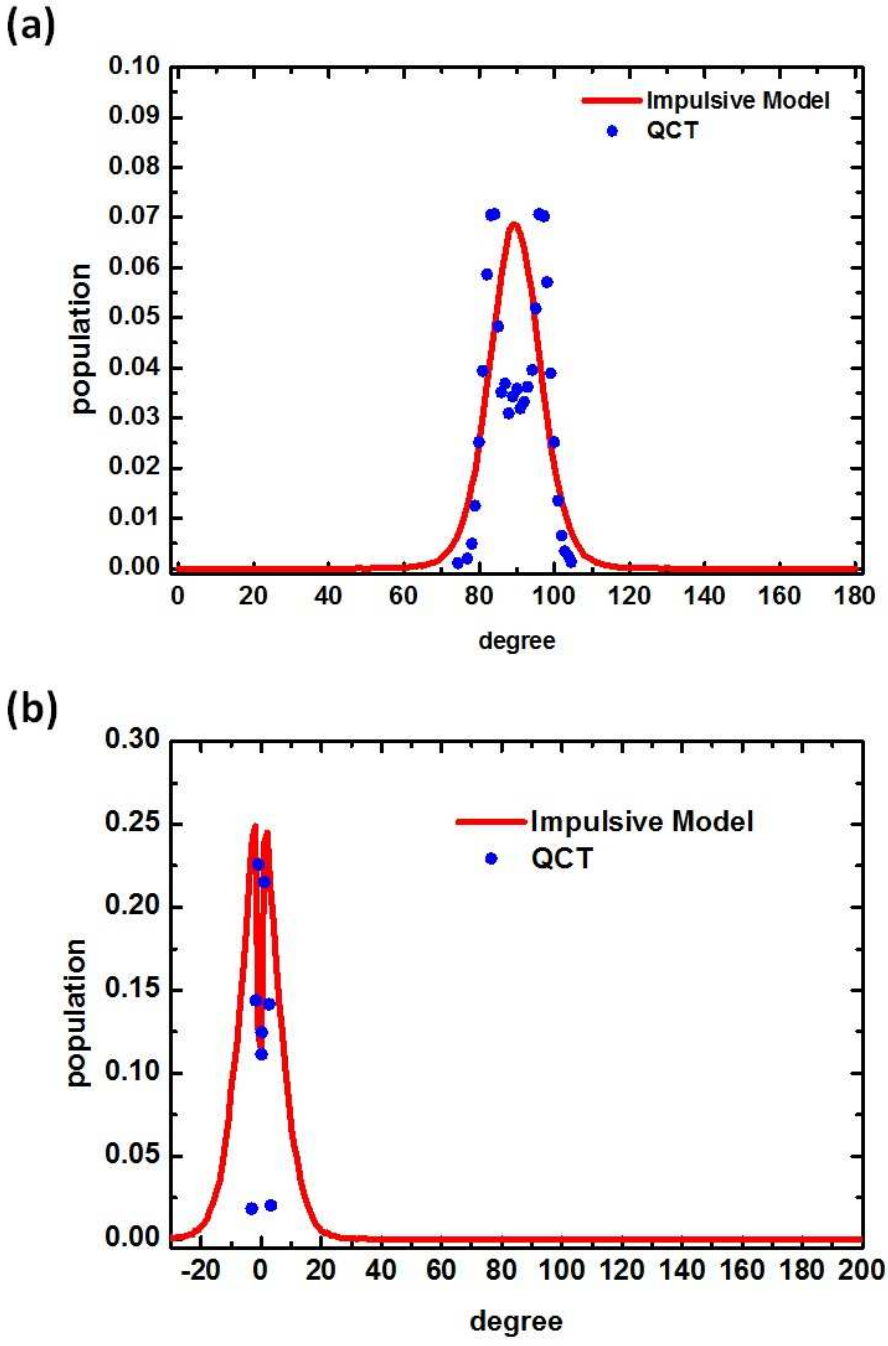

Fig.3

Physical Chemistry Chemical Physics Accepted Manuscript

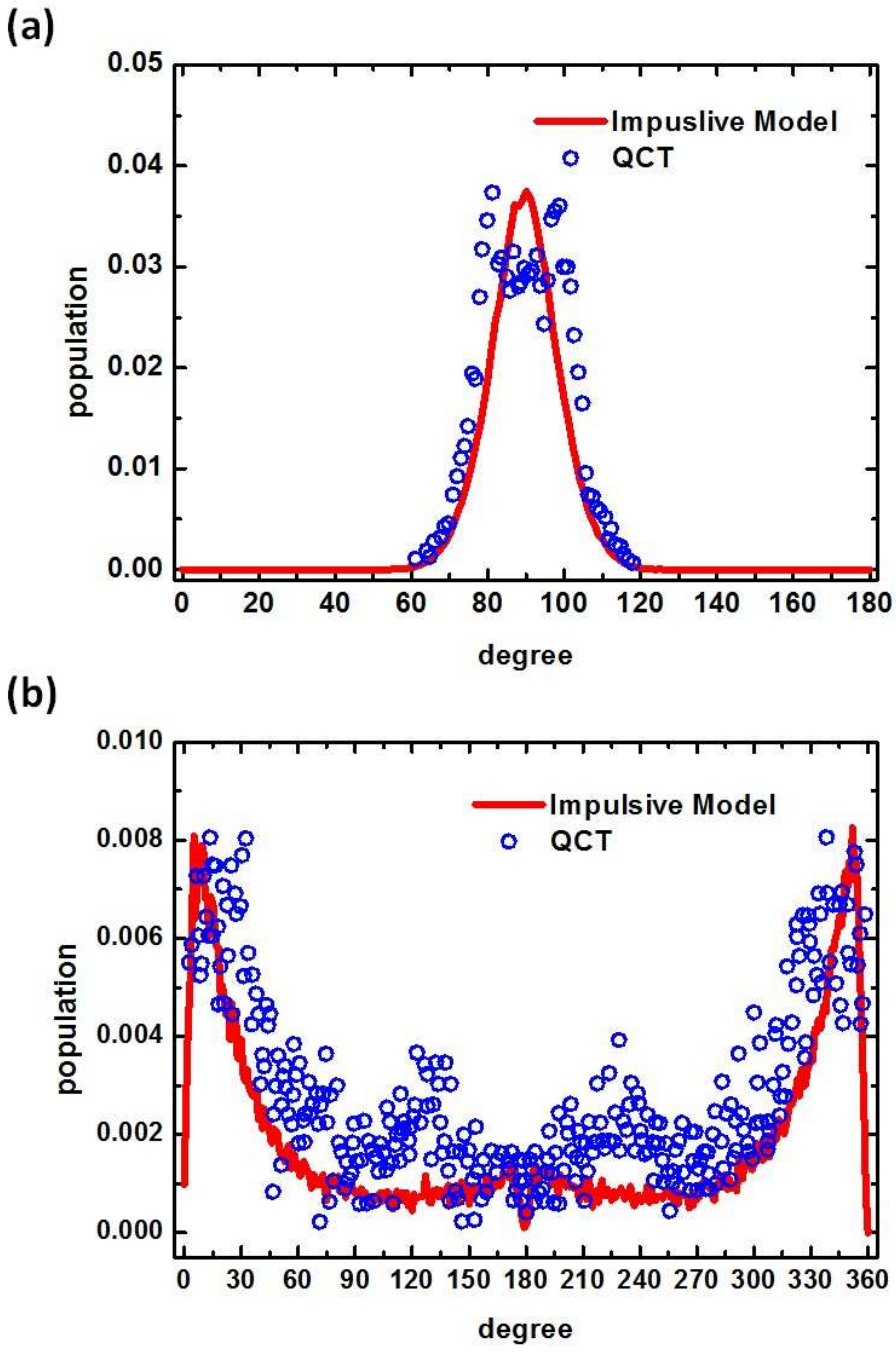

Fig.4

Physical Chemistry Chemical Physics Accepted Manuscript

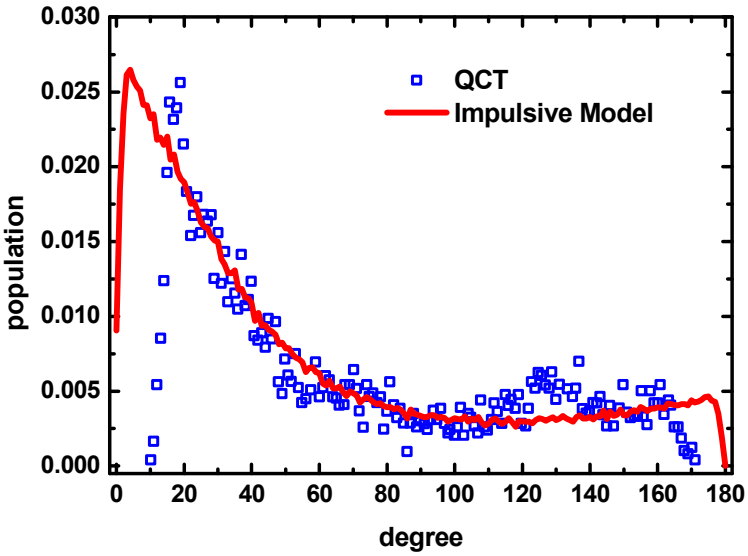

Fig.5

Physical Chemistry Chemical Physics Accepted Manuscript

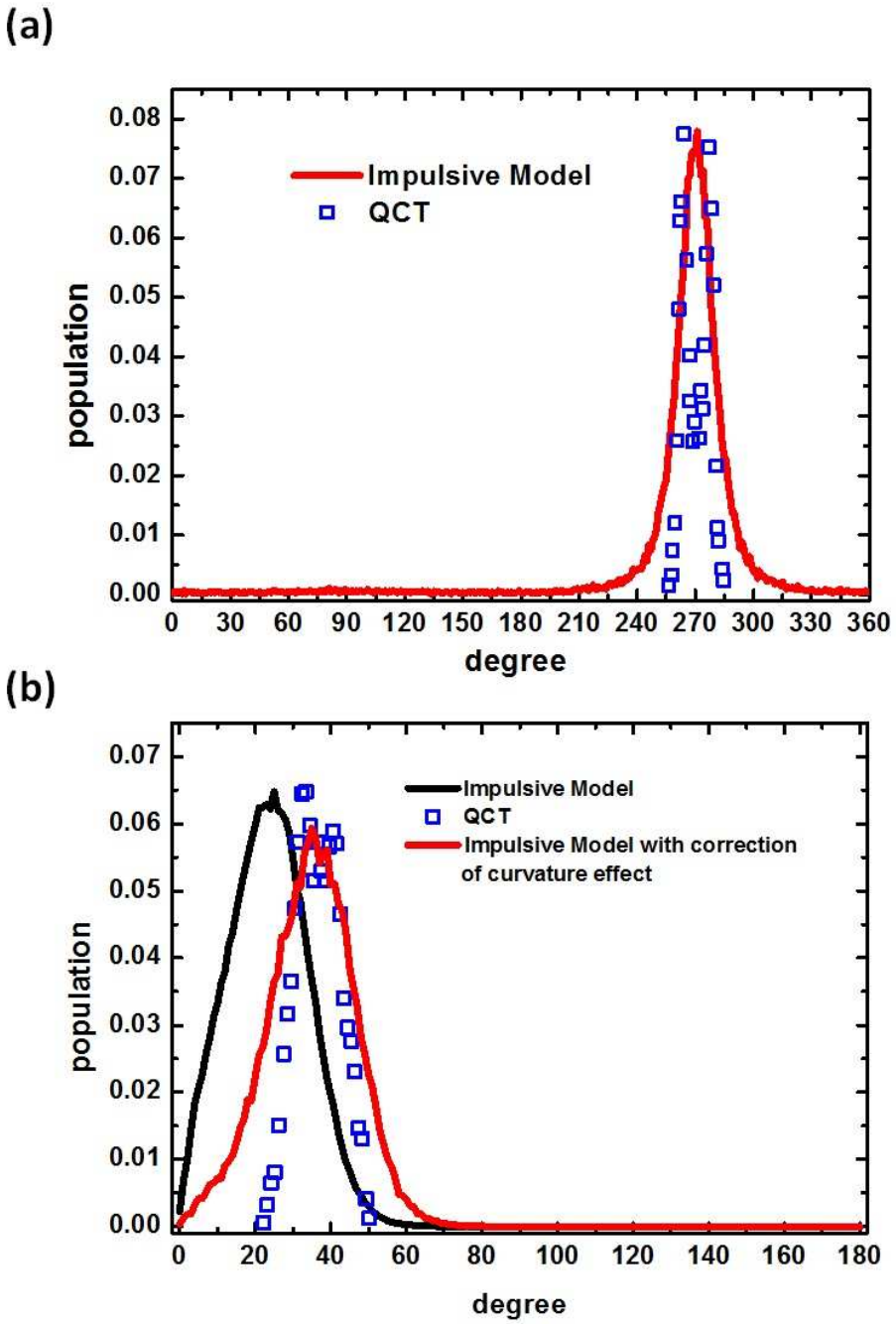

Fig.6

Physical Chemistry Chemical Physics Accepted Manuscript

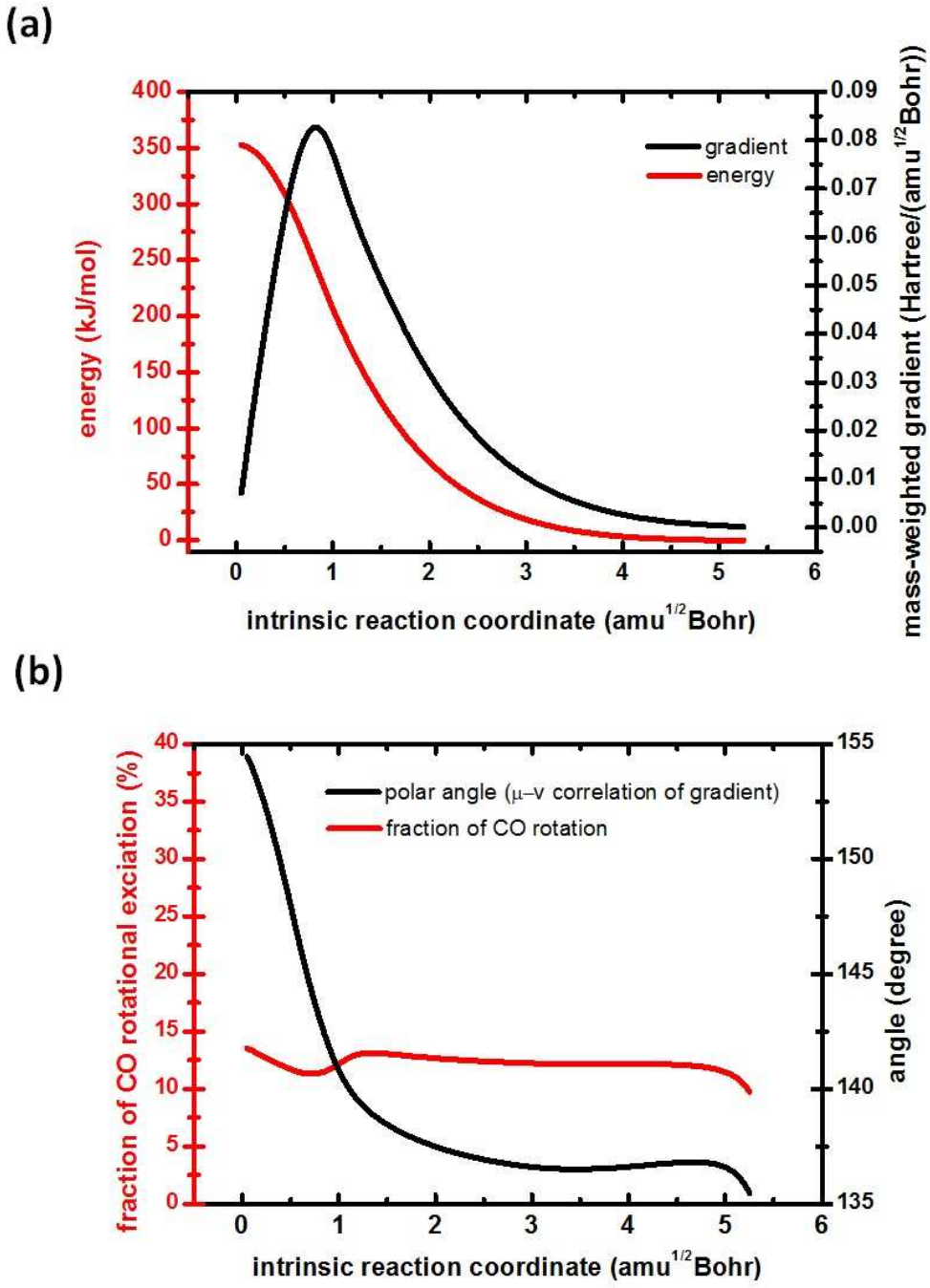

Fig.7

Physical Chemistry Chemical Physics Accepted Manuscript

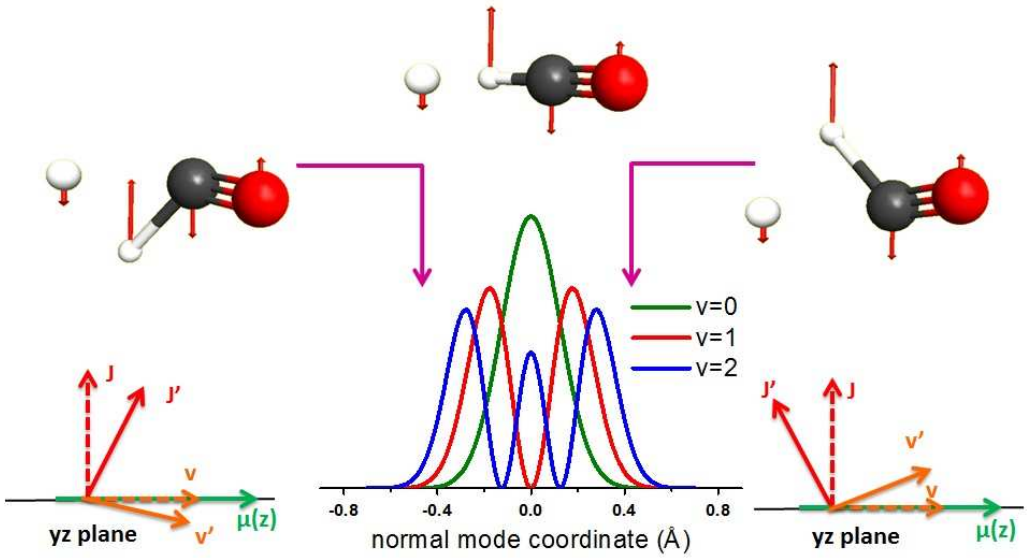

Fig.8

Physical Chemistry Chemical Physics Accepted Manuscript

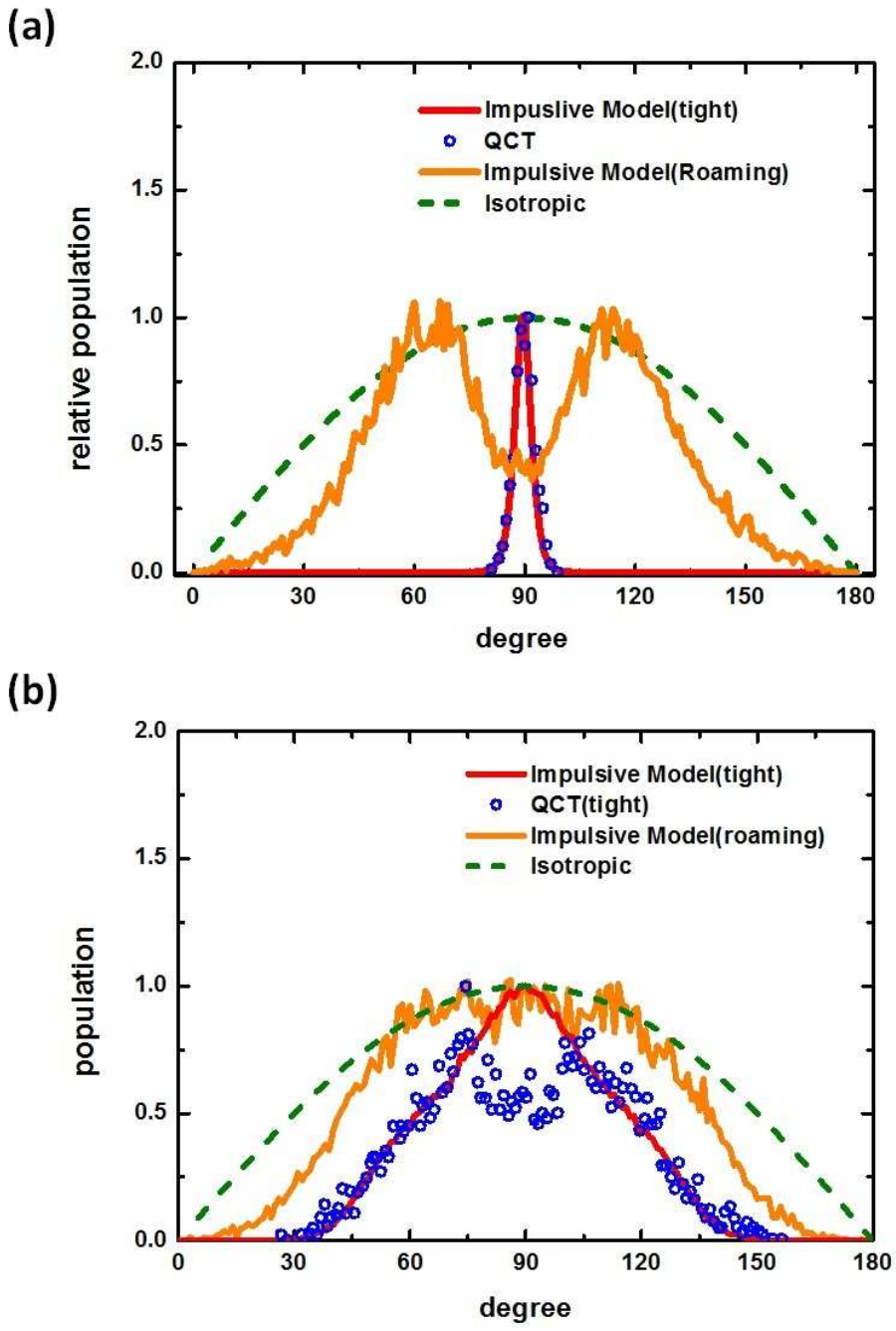

Fig.9

Physical Chemistry Chemical Physics Accepted Manuscript

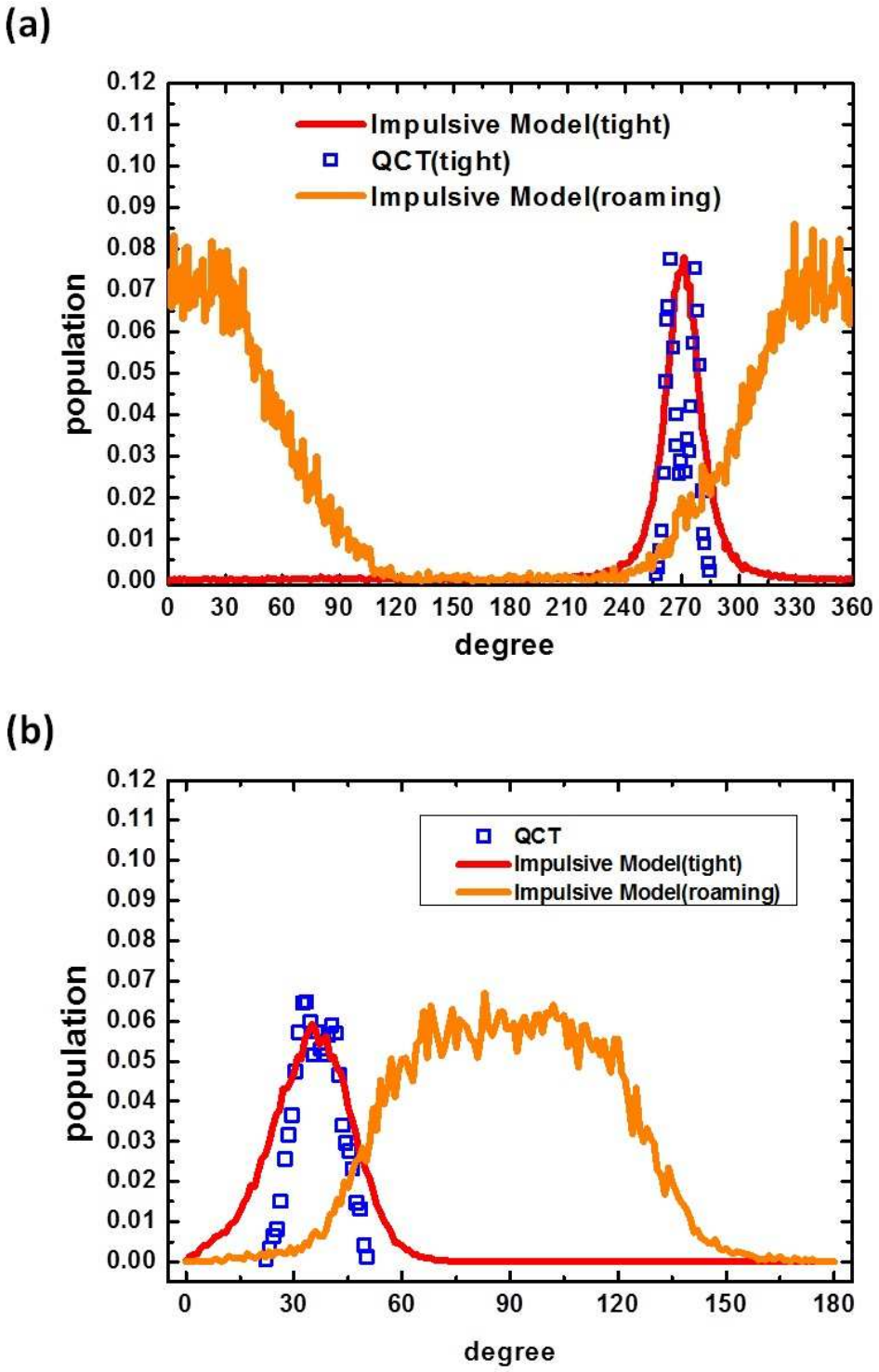

Fig.10

Physical Chemistry Chemical Physics Accepted Manuscript

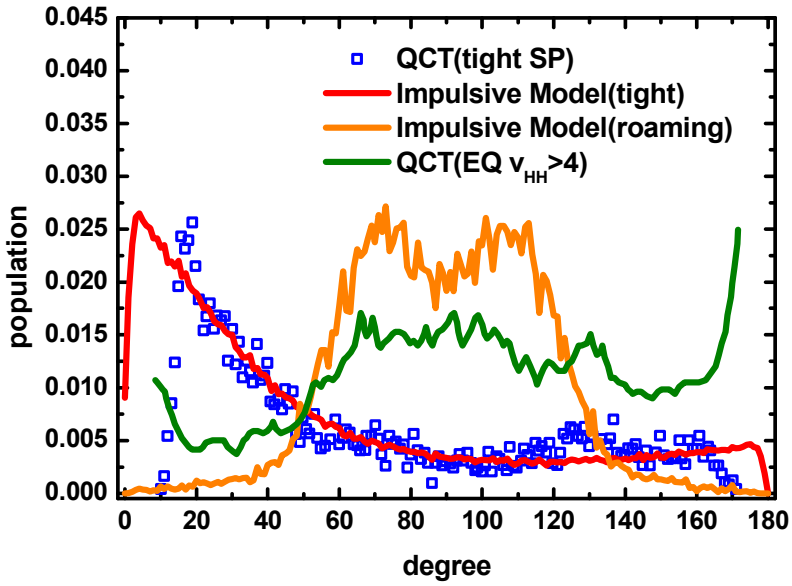

Fig.11

Physical Chemistry Chemical Physics Accepted Manuscript